Title

Direct utilization of gaseous fuels in metal supported solid oxide fuel cells

Journal

International Journal of Hydrogen Energy, 48(4)

ISSN

0360-3199

Authors

Welander, Martha M

Hu, Boxun

Belko, Seraphim

et al.

Publication Date

2023

DOI

10.1016/j.ijhydene.2022.10.008

Direct Utilization of Gaseous Fuels in Metal Supported Solid Oxide Fuel Cells

Martha Welander, Boxun Hu, Seraphim Belko, Kevin X. Lee, Pawan K. Dubey, Ian Robinson, Prabhakar Singh, Michael C. Tucker

Abstract

Direct utilization and internal reforming of gaseous fuels is investigated on symmetric-architecture metal supported solid oxide fuel cells (MS-SOFCs) with thin ceramic electrolyte and scaffold backbone layers, and low cost ferritic stainless steel supports on both sides. Infiltrated Pr-oxide and Ni/samarium-doped ceria catalysts are added to the cathode and anode electrodes, respectively. Initial performance and durability is evaluated for MS-SOFCs operating with natural gas, propane, ammonia, and dimethyl ether at 700 °C. Cells for natural gas and propane utilize a novel high entropy alloy (HEA) catalyst for internal reforming with performance and degradation rates similar to H_2 (0.5 W cm^{-2} and ~12% /100 h). Initial testing with sulfur shows reversible degradation for levels found in natural gas and irreversible degradation for higher levels found in commercial propane. Overall, MS-SOFCs show successful fuel flexibility.

MS-SOFC; Internal Reforming; High Entropy Alloy

*mctucker@lbl.gov

Phone 1-510-486-5304

Fax 1-510-486-4260

LBNL; 1 Cyclotron Rd; MS 62-203; Berkely CA 94720; USA

Introduction

Fuel cell systems can provide clean energy with high efficiencies by direct conversion of chemical energy into electricity. While hydrogen is the simplest and cleanest fuel, currently it is energetically expensive to produce, transport and store. High temperature solid oxide fuel cells (SOFCs) are capable of operating with other readily-available fuels. The availability of suitable fuel and an established refueling infrastructure is a pre-requisite for market introduction of fuel cells, giving fuel-flexible SOFCs a significant advantage [1]. Symmetric metal-supported SOFCs (MS-SOFCs) offer several advantages over conventional anode or electrolyte-supported SOFCs, including: inexpensive materials, rapid start-up capability, increased mechanical strength, and excellent tolerance to redox cycling.[2]–[4] MS-SOFCs show comparable performance to conventional cells (> 1 W cm^{-2}) with H_2 fuel [2], [5]–[7]. But while fuel flexibility of SOFCs is widely recognized, limited data is available for MS-SOFCs with internal reforming and direct utilization of non-hydrogen fuels. MS-SOFCs were operated with alternative fuels including reformed natural gas[8], [9], methane [10], ethanol[11], and propane in a direct-flame configuration [12]. While pre-reformed fuels minimize the amount of fuel conversion necessary at the anode, separate reforming processes upstream of the cell lower overall efficiencies.[13] Internal reforming and direct utilization simplifies system design by removing the requirement for a separate fuel reformer and significantly reduces the requirement for cell cooling, increasing efficiencies[14]. These benefits coupled with sparse literature on MS-SOFC fuel flexibility motivates this work.

SOFC operation is possible with ammonia, dimethyl ether (DME), natural gas, and propane. Ammonia is energy dense, carbon free at the point-of-use, and can be stored as a liquid at low pressures for transport [15]. While ammonia is currently produced by high-emission methods, ammonia can also be produced using green hydrogen. SOFCs operate with ammonia at a temperature that avoids formation of NOx [16]. Ammonia fuel is gaining attention as an SOFC fuel [17]–[20] but its use in MS-SOFCs is not yet reported.

SOFC operation with abundant hydrocarbon fuels is not emission-free, but provides a bridge to future energy infrastructure. Liquified hydrocarbons such as DME and propane offer straightforward handling and transport, while extensive infrastructure for natural gas already exists. With hydrocarbon fuels, MS-SOFCs are subject to the same limitations as conventional cells including risk of coking (carbon accumulation) on the anode surface, which impedes gas transport and blocks catalytic sites. Ni-based anode catalysts promote coking and therefore necessitate the use of upstream fuel reforming, increasing the complexity and cost of the system [13], [21]–[23]. An alternative approach is anode materials-based solutions that limit carbon accumulation. Alloys have higher thermodynamic barrier to carbon deposition than the constituent metals and are therefore obvious candidates for limiting coking.[24], While carbon tolerant non-Ni anode materials often severely sacrifice performance, Ni-based alloys show potential to resolve the tradeoff between performance and carbon tolerance, as they are expected to have high catalytic activity for hydrocarbon reforming from the Ni metal and good carbon tolerance from the secondary metal properties [25]. Cu, Co, and Fe have shown promise in their ability to operate directly with hydrocarbon fuels without coking [26]–[29]. These elements are not as catalytic as Ni, but can still aid electronic conductivity [27], [30]. High entropy alloys (HEA), also known as multi-constituent alloys, contain 5 metals of close to equi-atomic ratios, with improved mechanical and catalytic properties. HEA electrodes can be tailored by combining highly active Ni with elements that have a high affinity for oxygen to minimize carbon deposition. The catalytic activity can also be intentionally moderated to spread the endothermic reforming reaction over a larger cell area, thereby mitigating rapid cooling at the cell or stack inlet. By slowing down the rate of reformation and adsorbing more oxygen to the catalyst surface, HEAs can provide excellent chemical and structural stability while continuously converting hydrocarbon fuels to hydrogen.[[31]–[33]

Carbon-based fuels often contain impurities such as sulfur, chlorine, silicone and phosphorous. Sulfur poisoning can accelerate degradation of SOFCs through several different mechanisms. Short term effects include fast physisorption and chemisorption of sulfur with a deactivation of the triple phase boundary and long term effects may include structural modifications and nickel migration [24], [34], [35].

Desulfurizers are used to decrease risk of material degradation and performance loss, but add cost and complexity [36]. The impact of sulfur-contaminated externally reformed fuel on SOFC anode materials in real electrodes is not well studied, nor is the impact of sulfur on MS-SOFCs.

This study successfully demonstrates fuel flexibility of MS-SOFCs. Natural gas and propane (with and without sulfur) are reformed with a novel on-cell HEA catalyst, and dimethyl ether and ammonia are utilized directly. To the authors knowledge, these findings are some of the first to explore direct internal reforming and utilization of these fuels with MS-SOFCs, and the use of HEAs with MS-SOFCs.

Materials and methods

MS-SOFCs consisting of thin ceramic scandia-ceria-stabilized zirconia (ScSZ) electrolytes, ScSZ scaffold backbone layers with infiltrated catalysts, and ferritic stainless steel supports were used for this work and prepared with techniques reported previously [37]. Laminated green tapes were laser cut (Hobby model, Full Spectrum Laser) into button cells that were de-binded in air at 525 °C for 1h and sintered at 1350 °C for 2 h in 2 % H_2 in Ar, and pre-oxidized in air at 850 °C for 10 h. Resulting cells were ~26 mm in diameter.

Cells were infiltrated by masking the edges with acrylic paint (Liquitex) and infiltrating with metal nitrate catalyst precursor solutions under vacuum. Catalyst solutions were prepared by mixing stoichiometric amounts of metal nitrates with Triton-X 100 (both Sigma Aldrich) in water to a total metal nitrate concentration of 3.3 M and 3.7 M for the cathode and anode, respectively. The cathode electrocatalyst was Pr_6O_{11} (PrOx) and the anode catalyst was 40 vol% Ni-60vol% $Sm_{0.2}Ce_{0.8}O_{2-\delta}$ (SDCN40). Cathode and anode catalysts were infiltrated 10 times each and fired at 800 °C in air for 30 minutes between infiltrations to convert the precursors into the appropriate oxide phases. SEM images of the catalysts and cell structure are available in Refs [11], [38].

HEA containing Ni, Co, Cu, Fe, and Mn was prepared using the co-precipitation method by dissolving metal nitrates and citric acid in DI water, in a 1:1 citric acid:metal molar ratio. Additionally, gadolinium-doped ceria powder (GDC-10, Fuel Cell Materials) was added to the solution as an ion conductor for the catalyst, with the final mass ratio of metallic HEA to GDC-10 being 65:35wt%. After raising the pH of the solution to 7 to 9 using ammonium hydroxide, the solution was dried overnight to leave a gel that was calcined at 750^{o}C in air overnight. The resulting powder was milled in a planetary ball mill to reduce particle size for good catalytic performance. For some cells, a precursor solution of HEA was added to the interior of the anode through infiltration and fired using identical methods as the PrOx and SDCN40 catalysts. Then a thin (~20 μm) layer of HEA ink was painted onto the surface of the anode using a brush and the cell was heated to 800 °C for 1 h to assure firm attachment of this catalyst layer.

Platinum wires and mesh were spot welded onto the electrodes for electrical connection. Cells were sealed onto 410 stainless steel rigs using glass paste (80 wt% glass powder, GM31107 Schott and 20 wt% ink vehicle, Fuel Cell Materials). Test rigs were placed inside tube furnaces and heated to 90 °C at 10° C/min, 200 °C at 2°C/min, and to 700 °C at 10 °C/min. Cathodes were exposed to static air and anodes were flushed with N_2 followed by initial reduction in humidified H_2 (3% H_2O) at a 100 sccm flow rate. Cells were considered fully reduced when the open circuit voltage (OCV) stabilized ~1.10 V. Catalyst pre-coarsening was performed at 750 °C for 4 h prior to initiating testing at 700 °C. Simulated natural gas (Praxair: 93.01% methane, 4 % ethane, 0.4 % propane, 0.06 % N-butane, 0.02 % n-pentane, 0.01 % n-hexane, 2 % nitrogen and 0.5 % carbon dioxide) was delivered through a heated water bubbler and heat-traced lines to produce 20% H_2O. For natural gas experiments with sulfur, 75 ppm H_2S in H_2 was added to the fuel stream through a mixing tube in the hot zone of the test rig. Standard commercial (BBQ) odorized propane was delivered through a desulfurizer (SulfaTrap) and mixed with air to produce a 1.5:1 O:C ratio. The propane desulfurizer was removed to test sulfur tolerance at the end of the experiment. Dimethyl ether and ammonia were delivered at cylinder purity directly to the cells.

Electrochemical measurements were performed with a VMP3 multi-channel potentiostat and current booster (Biologic). Linear sweep voltammetry (LSV) recorded the I-V polarization curve with a sweep rate of 10 mV/s between voltage limits of 100% and 30% of the measured OCV in order to avoid cell damage at very low voltage. Electrochemical impedance spectroscopy (EIS) measurements were collected at open circuit with an AC voltage amplitude of 5 mV over a frequency range of 200 kHz to 100 mHz.

Bench-top experiments were performed in a fixed-bed quartz tubular reactor (0.5" OD) with sample powders prepared in-house. Approximately 0.1 g of the anode catalyst was supported at the center of the reactor using quartz wool supports on both sides. The catalyst was first reduced in a flowing N_2- 4% H_2 gas at 700 ˚C for 2 h. A methane - steam gas mixture was heated in an evaporator at 120 ˚C and the evaporated gas mixture was subsequently allowed to flow at 30 SCCM into the reactor. The exhaust gas was collected and analyzed using a SRI 8610 gas chromatograph equipped with a helium ionization detector (HID). The conversion of methane was observed for 30 h. Upon completion of the experiment, the reactor was purged with nitrogen, followed by H_2 gas flow from operating temperature to room temperature. Post-test samples were collected and further analyzed for carbon deposition using a Renishaw System 2000 Raman spectrometer.

Results and Discussion

The performance and initial durability of MS-SOFCs operating with natural gas, ammonia, dimethyl ether (DME) and propane were assessed and compared to H_2 baseline. For natural gas and propane, a HEA internal reforming catalyst combining Ni, Co, Cu, Fe, and Mn was added to the anode. The internal reforming catalyst enables reforming primarily on the anode support, followed by fuel oxidation by the anode electrocatalytic electrode layer [39]. DME and ammonia did not require the addition of a HEA since fuel cracking occurs spontaneously at the operating temperature [40], [41].

The catalytic activity of HEA/GDC for reforming of humidified methane was assessed using a fixed-bed reactor, and compared to Ni/YSZ and Ni/GDC baseline catalysts, Figure 1. The testing temperature of 600°C was chosen to illustrate the difference in carbon deposition between Ni and HEA. The steam-to-carbon ratio (S/C) was 2 and the total gas space velocity was calculated to be approximately 45,000 h^{-1}. Ni/YSZ and Ni/GDC catalytic performance degraded noticeably with time due to carbon corrosion, while HEA/GDC showed stable performance over 30 h. The HEA/GDC also provided moderate performance, as intended to tailor the reforming endotherm. Raman spectra of the post-test catalysts reveal amorphous (~1350 cm^{-1}) and graphitic carbon (~1600 cm^{-1}) deposits on the surfaces of both Ni/YSZ and Ni/GDC. No carbon was detected on the surface of HEA/GDC catalysts, owing to the increased activation energy for carbon formation achieved by alloying Ni with the other transition metals.

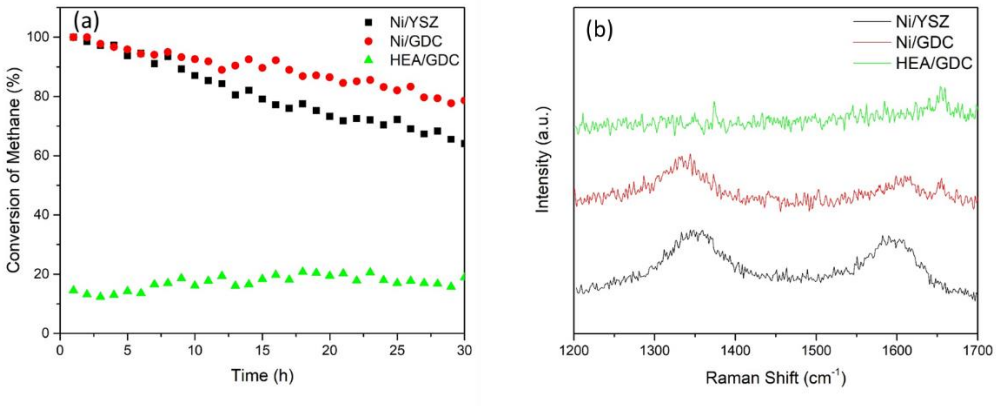

Figure 1. HEA initial assessment. (a) Methane conversion in a fixed-bed reactor at 600°C for Ni/YSZ (65/35wt) (black), Ni/GDC (50/50wt) (red), and HEA/GDC (65/35wt) (green). (b) Raman spectroscopy of post-test catalysts after 30 h time-on-stream**.**

Reforming on various candidate cell designs was first screened with methane fuel, Figure 2. The HEA catalyst enhanced internal reforming, increasing both initial performance and durability. Addition of the catalyst through a combination of infiltration and ink showed superior peak power density of 0.5 W cm^{-2} compared to ~0.3 W cm^{-2} and 0.25 W cm^{-2} when added through only infiltration or ink, respectively,

Figure 2a. The HEA provided a dramatic improvement over a standard MS-SOFC and one with an additional layer of NiO ink on the anode, Figure 2b. All cells experienced the majority of degradation in the first 10 h, likely from initial carbon deposition, and the HEA cell maintains much higher performance throughout. Carbon accumulation was visible on standard cells after CH_4 exposure, but not on the cells with HEA. This implies that HEA provides higher thermodynamic barrier to carbon deposition and increases internal reforming capability. Because internal reforming is negligible in the metal support itself [42], the addition of HEA is thought to benefit reforming on both the anode electrode and support layers. Based on these results, infiltrated and ink HEA was chosen as the reforming catalyst for demonstration with other fuels.

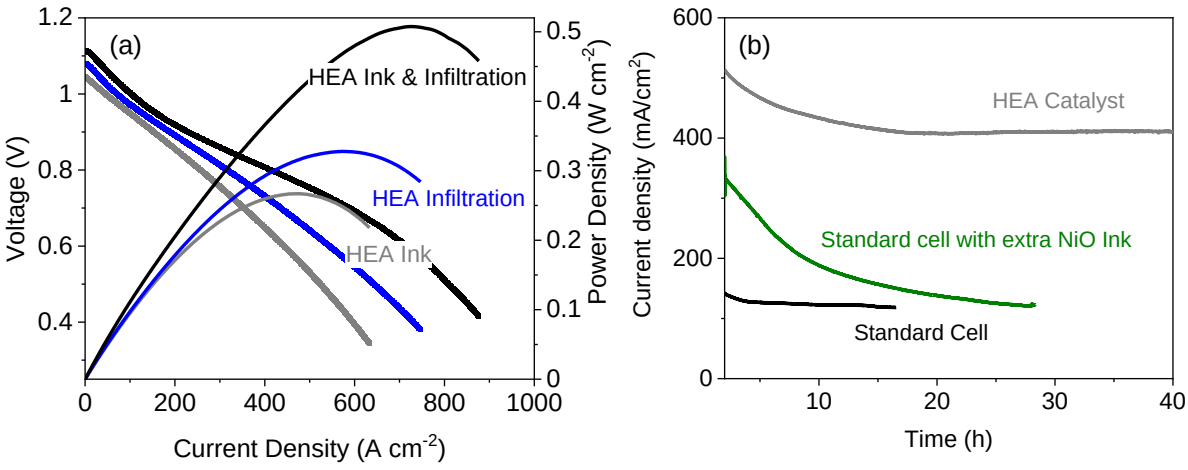

Figure 2. Hydrocarbon fuel reforming catalyst screening with CH_4 in 3 % H_2O. (a) Performance of MS-SOFC with HEA reforming catalyst added via infiltration, ink, and a mixture of both at 700 °C. (b) Initial potentiostatic operation of MS-SOFC with standard SDCN catalyst, extra NiO, or HEA ink and infiltration at 750 °C and 0.75 V.

MS-SOFC performance with ammonia, propane, DME and natural gas were broadly similar to baseline performance with H_2, Figure 3a. The OCV was reduced for propane due to the increased partial pressure of oxygen from air added to promote partial oxidation reforming. Ammonia was delivered to the cell dry and the measured OCV was therefore closer to 1.2 V. Fuel compositional changes due to the addition of

electrochemical oxygen are also expected to have an effect as the current density increases. The apparent mass transport limit at high current density arises from oxygen concentration polarization in the cathode and is currently under investigation. Peak power density was higher with natural gas and propane, and lower for DME and ammonia. Ohmic resistance was similar for all fuels, based on normal cell-to cell variation, with a small decrease for natural gas and propane, Figure 3b. This is speculated to arise from improved electronic conductivity in the anode due to the additional HEA. The polarization resistance increases dramatically with natural gas, possibly stemming from carbon formation and competition between reforming and electrochemical reactions at the anode due to the presence of C4 to C6 hydrocarbons. Increased polarization resistance was not observed for propane, likely due the increased O:C ratio and lower molecular weight preventing carbon formation.[43] As expected, ammonia and DME cracked to provide sufficient hydrogen to support the electrochemical reaction.

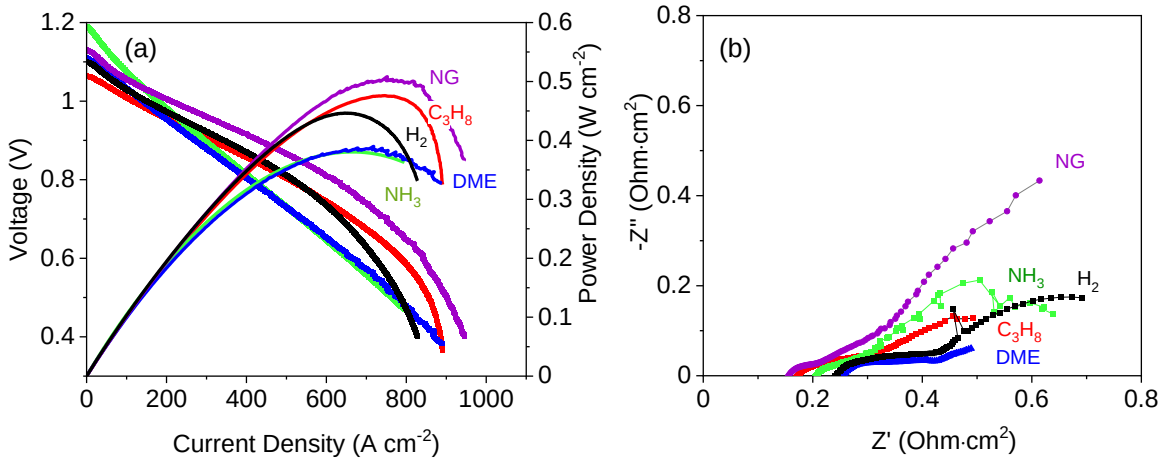

Figure 3. Performance with various fuels. (a) Polarization behavior and (b) EIS of cells operating with hydrogen (H_2), natural gas (NG), propane (C_3H_8), dimethyl ether (DME) and ammonia (NH_3) at 700 °C.

MS-SOFCs were operated successfully for 200 h with natural gas, ammonia and propane. Degradation rates were similar to H_2 for all fuels and ranged between 12 to 15 %/100 h, Figure 4. With H_2

and pre-reformed natural gas fuels, degradation is known to be dominated by Ni coarsening in the anode and Cr deposition in the cathode, both of which contribute to an increase in polarization impedance[38], [44]. For multiple cells operating with hydrocarbon fuels and added HEA, a transient break-in period was observed for 25 to 50 h, presumably due to evolution of the HEA catalyst. This was followed by more steady performance. Carbon formation was visually observed post mortem on the outer surface of the anode for both natural gas and propane. Nitriding of the metal support from ammonia exposure was not of observed based on absence of changes in the XRD pattern post mortem (not shown). EIS after operation shows the degradation is dominated by increased polarization resistance, consistent with the mechanisms listed above (Figure 4d, compare to fresh cells in Figure 3b). Longer-term operation and detailed post-mortem analysis is the subject of future work.

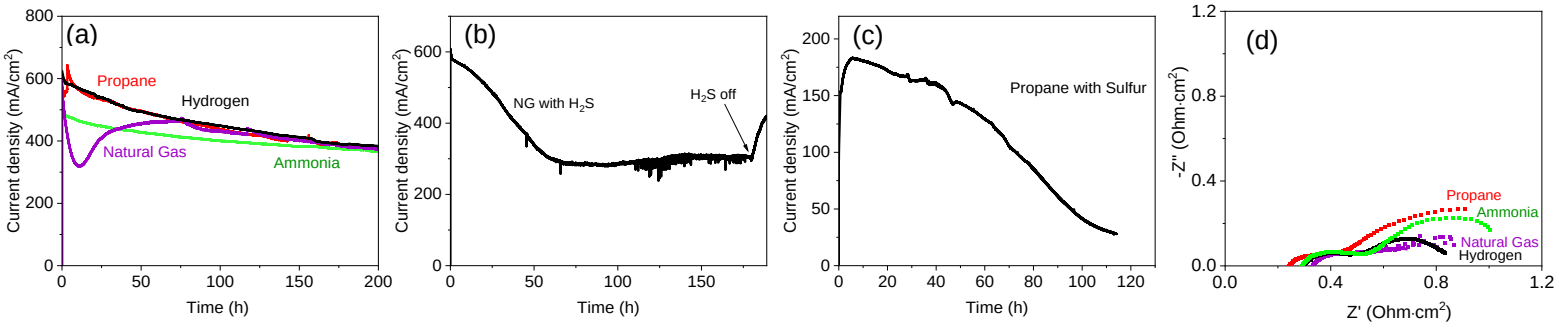

Figure 4. Cell degradation behavior at 0.75 V. Degradation of cells operating with (a) internal reforming (without sulfur) and direct utilization of various fuels at 700 °C, (b) natural gas with 5 ppm H_2S at 700 °C and (c) commercial propane with sulfur at 750 °C and 0.75 V. (d) EIS at OCV after the 200 h operation shown in in (a).

The presence of sulfur in hydrocarbon fuels significantly impacted performance, Figures 4b,c. For natural gas, sulfur was added by mixing 5 ppm H_2S into the fuel stream, a level that is representative of pipeline natural gas. Increased degradation was observed for the first 50 h with subsequent stabilization at 50% of the initial current density, Figure 4b. Our recent study demonstrated that the MS-SOFC anode electrochemical reactions are tolerant to 5 ppm sulfur in pre-reformed natural gas mixtures [38], so we

speculate that adsorption of sulfur on HEA limits the reforming reaction and explains the behavior seen here. About half of the decreased performance was found to be reversible upon removal of sulfur from the fuel stream, with recovery to about 450 mA cm^{-2}. For propane, significantly higher concentration of sulfur is present and was allowed to reach the cell by removing the desulfurizer trap. This high sulfur concentration led to quick and irreversible degradation of the cell, Figure 4c. The cell failed, so testing was stopped.

Conclusion

MS-SOFCs were successfully operated with a variety of alternative fuels including natural gas, ammonia, propane and DME. A HEA catalyst added to the anode provided excellent reforming of humidified natural gas and propane mixed with air. Cells operated for 200 h with natural gas, propane, and ammonia showed similar degradation rates to H_2 baseline, suggesting the presence of the additional fuel components, the HEA, and reforming reaction do not introduce significant new degradation mechanisms. Addition of sulfur to propane and natural gas fuels led to quick degradation, with reversibility possible for the 5 ppm H_2S added to natural gas. This work demonstrates the ability of MS-SOFCs to operate with commercially-available fuels using direct internal reforming and utilization for cases where hydrogen is not available or preferred.

Acknowledgments:

We thank Jeff Chase, Greg Tao and Michael King for helpful discussion. This work was funded in part by the Southern California Gas Company (SoCalGas), a public utility company. This work was funded in part by the U.S. Department of Energy under contract no. DE-AC02-05CH11231. The views and opinions of the authors expressed herein do not necessarily state or reflect those of the United States Government or any agency thereof. Neither the United States Government nor any agency thereof, nor any of their employees, makes any warranty, expressed or implied, or assumes any legal liability or responsibility for

the accuracy, completeness, or usefulness of any information, apparatus, product, or process disclosed, or represents that its use would not infringe privately owned rights.

References

[1] A. Weber, "Fuel flexibility of solid oxide fuel cells," *Fuel Cells*, vol. 21, no. 5, pp. 440–452, 2021, doi: 10.1002/fuce.202100037.

[2] M. C. Tucker, "Progress in metal-supported solid oxide fuel cells: A review," *J. Power Sources*, vol. 195, no. 15, pp. 4570–4582, Aug. 2010, doi: 10.1016/j.jpowsour.2010.02.035.

[3] V. V. Krishnan, "Recent developments in metal-supported solid oxide fuel cells," *WIREs Energy Environ.*, vol. 6, no. 5, p. e246, 2017, doi: 10.1002/wene.246.

[4] Y. Larring and M.-L. Fontaine, "Critical Issues of Metal-Supported Fuel Cell," in *Solid Oxide Fuels Cells: Facts and Figures: Past Present and Future Perspectives for SOFC Technologies*, J. T. S. Irvine and P. Connor, Eds. London: Springer, 2013, pp. 71–93. doi: 10.1007/978-1-4471-4456-4_4.

[5] P. Blennow *et al.*, "Development of Planar Metal Supported SOFC with Novel Cermet Anode," *ECS Trans.*, vol. 25, no. 2, pp. 701–710, Dec. 2019, doi: 10.1149/1.3205585.

[6] T. Klemenso *et al.*, "Development of Long-Term Stable and High-Performing Metal-Supported SOFCs," *ECS Trans.*, vol. 35, no. 1, pp. 369–378, Dec. 2019, doi: 10.1149/1.3570011.

[7] J. Nielsen, Å. H. Persson, T. T. Muhl, and K. Brodersen, "Towards High Power Density Metal Supported Solid Oxide Fuel Cell for Mobile Applications," *J. Electrochem. Soc.*, vol. 165, no. 2, pp. F90–F96, 2018, doi: 10.1149/2.0741802jes.

[8] R. T. Leah *et al.*, "Ceres Power Steel Cell Technology: Rapid Progress Towards a Truly Commercially Viable SOFC," *ECS Trans.*, vol. 68, no. 1, pp. 95–107, Jul. 2015, doi: 10.1149/06801.0095ecst.

[9] R. T. Leah *et al.*, "Latest Results and Commercialization of the Ceres Power SteelCell® Technology Platform," *ECS Trans.*, vol. 91, no. 1, pp. 51–61, Jul. 2019, doi: 10.1149/09101.0051ecst.

[10] J. O. Christensen, A. Hagen, and B. R. Sudireddy, "Performance of Metal Supported SOFCs Operated in Hydrocarbon Fuels and at Low (<650˚C) Temperatures," *ECS Trans.*, vol. 103, no. 1, pp. 713–724, Jul. 2021, doi: 10.1149/10301.0713ecst.

[11] E. Dogdibegovic, Y. Fukuyama, and M. C. Tucker, "Ethanol internal reforming in solid oxide fuel cells: A path toward high performance metal-supported cells for vehicular applications," *J. Power Sources*, vol. 449, p. 227598, Feb. 2020, doi: 10.1016/j.jpowsour.2019.227598.

[12] M. C. Tucker and A. S. Ying, "Metal-supported solid oxide fuel cells operated in direct-flame configuration," *Int. J. Hydrog. Energy*, vol. 42, no. 38, pp. 24426–24434, Sep. 2017, doi: 10.1016/j.ijhydene.2017.07.224.

[13] H. He and J. M. Hill, "Carbon deposition on Ni/YSZ composites exposed to humidified methane," *Appl. Catal. Gen.*, vol. 317, no. 2, pp. 284–292, Feb. 2007, doi: 10.1016/j.apcata.2006.10.040.

[14] P. Aguiar, C. S. Adjiman, and N. P. Brandon, "Anode-supported intermediate-temperature direct internal reforming solid oxide fuel cell: II. Model-based dynamic performance and control," *J. Power Sources*, vol. 147, no. 1, pp. 136–147, Sep. 2005, doi: 10.1016/j.jpowsour.2005.01.017.

[15] G. Cinti, G. Discepoli, E. Sisani, and U. Desideri, "SOFC operating with ammonia: Stack test and system analysis," *Int. J. Hydrog. Energy*, vol. 41, no. 31, pp. 13583–13590, Aug. 2016, doi: 10.1016/j.ijhydene.2016.06.070.

[16] A. Afif, N. Radenahmad, Q. Cheok, S. Shams, J. H. Kim, and A. K. Azad, “Ammonia-fed fuel cells: a comprehensive review,” *Renew. Sustain. Energy Rev.*, vol. 60, pp. 822–835, Jul. 2016, doi: 10.1016/j.rser.2016.01.120.
[17] A. Fuerte, R. X. Valenzuela, M. J. Escudero, and L. Daza, “Ammonia as efficient fuel for SOFC,” *J. Power Sources*, vol. 192, no. 1, pp. 170–174, Jul. 2009, doi: 10.1016/j.jpowsour.2008.11.037.
[18] S. S. Rathore, S. Biswas, D. Fini, A. P. Kulkarni, and S. Giddey, “Direct ammonia solid-oxide fuel cells: A review of progress and prospects,” *Int. J. Hydrog. Energy*, vol. 46, no. 71, pp. 35365–35384, Oct. 2021, doi: 10.1016/j.ijhydene.2021.08.092.
[19] Z. Wan, Y. Tao, J. Shao, Y. Zhang, and H. You, “Ammonia as an effective hydrogen carrier and a clean fuel for solid oxide fuel cells,” *Energy Convers. Manag.*, vol. 228, p. 113729, Jan. 2021, doi: 10.1016/j.enconman.2020.113729.
[20] B. Stoeckl *et al.*, “Characterization and performance evaluation of ammonia as fuel for solid oxide fuel cells with Ni/YSZ anodes,” *Electrochimica Acta*, vol. 298, pp. 874–883, Mar. 2019, doi: 10.1016/j.electacta.2018.12.065.
[21] G. J. Offer, J. Mermelstein, E. Brightman, and N. P. Brandon, “Thermodynamics and Kinetics of the Interaction of Carbon and Sulfur with Solid Oxide fuel Cell Anodes,” *J. Am. Ceram. Soc.*, vol. 92, no. 4, pp. 763–780, 2009, doi: 10.1111/j.1551-2916.2009.02980.x.
[22] Z. Tao, G. Hou, N. Xu, and Q. Zhang, “A highly coking-resistant solid oxide fuel cell with a nickel doped ceria: Ce1−xNixO2−y reformation layer,” *Int. J. Hydrog. Energy*, vol. 39, no. 10, pp. 5113–5120, Mar. 2014, doi: 10.1016/j.ijhydene.2014.01.092.
[23] H. Li, Y. Tian, Z. Wang, F. Qie, and Y. Li, “An all perovskite direct methanol solid oxide fuel cell with high resistance to carbon formation at the anode,” *RSC Adv.*, vol. 2, no. 9, pp. 3857–3863, Apr. 2012, doi: 10.1039/C2RA01256A.
[24] P. Boldrin, E. Ruiz-Trejo, J. Mermelstein, J. M. Bermúdez Menéndez, T. Ramírez Reina, and N. P. Brandon, “Strategies for Carbon and Sulfur Tolerant Solid Oxide Fuel Cell Materials, Incorporating Lessons from Heterogeneous Catalysis,” *Chem. Rev.*, vol. 116, no. 22, pp. 13633–13684, Nov. 2016, doi: 10.1021/acs.chemrev.6b00284.
[25] S. Kim, C. Kim, J. H. Lee, J. Shin, T.-H. Lim, and G. Kim, “Tailoring Ni-based catalyst by alloying with transition metals (M=Ni, Co, Cu, and Fe) for direct hydrocarbon utilization of energy conversion devices.,” *Electrochimica Acta*, vol. 225, pp. 399–406, Jan. 2017, doi: 10.1016/j.electacta.2016.12.178.
[26] J. H. Park *et al.*, “Boosting the Performance of Solid Oxide Electrolysis Cells via Incorporation of Gd3+ and Nd3+ Double-doped Ceria ▲,” *Fuel Cells*, vol. 20, no. 6, pp. 712–717, 2020, doi: https://doi.org/10.1002/fuce.201900248.
[27] H. Kim, C. Lu, W. L. Worrell, J. M. Vohs, and R. J. Gorte, “Cu-Ni Cermet Anodes for Direct Oxidation of Methane in Solid-Oxide Fuel Cells,” *J. Electrochem. Soc.*, vol. 149, no. 3, p. A247, Jan. 2002, doi: 10.1149/1.1445170.
[28] O. A. Marina, C. Bagger, S. Primdahl, and M. Mogensen, “A solid oxide fuel cell with a gadolinia-doped ceria anode: preparation and performance,” *Solid State Ion.*, vol. 123, no. 1, pp. 199–208, Aug. 1999, doi: 10.1016/S0167-2738(99)00111-3.
[29] T. D. McColm and J. T. S. Irvine, “B site doped strontium titanate as a potential SOFC substrate,” *Ionics*, vol. 7, no. 1, pp. 116–121, Jan. 2001, doi: 10.1007/BF02375477.
[30] M. F. Rabuni, T. Li, P. Punmeechao, and K. Li, “Electrode design for direct-methane micro-tubular solid oxide fuel cell (MT-SOFC),” *J. Power Sources*, vol. 384, pp. 287–294, Apr. 2018, doi: 10.1016/j.jpowsour.2018.03.002.
[31] E. P. George, D. Raabe, and R. O. Ritchie, “High-entropy alloys,” *Nat. Rev. Mater.*, vol. 4, no. 8, Art. no. 8, Aug. 2019, doi: 10.1038/s41578-019-0121-4.

[32] M. F. Serincan, U. Pasaogullari, and P. Singh, “Controlling reformation rate for a more uniform temperature distribution in an internal methane steam reforming solid oxide fuel cell,” *J. Power Sources*, vol. 468, p. 228310, Aug. 2020, doi: 10.1016/j.jpowsour.2020.228310.
[33] P. Singh, R. J. Ruka, and R. A. George, “Direct utilization of hydrocarbon fuels in high temperature solid oxide electrolyte fuel cells,” in *Proceedings of the 24th Intersociety Energy Conversion Engineering Conference*, Aug. 1989, pp. 1553–1563 vol.3. doi: 10.1109/IECEC.1989.74676.
[34] D. Papurello, A. Lanzini, S. Fiorilli, F. Smeacetto, R. Singh, and M. Santarelli, “Sulfur poisoning in Ni-anode solid oxide fuel cells (SOFCs): Deactivation in single cells and a stack,” *Chem. Eng. J.*, vol. 283, pp. 1224–1233, Jan. 2016, doi: 10.1016/j.cej.2015.08.091.
[35] A. Weber, S. Dierickx, A. Kromp, and E. Ivers-Tiffée, “Sulfur Poisoning of Anode-Supported SOFCs under Reformate Operation,” *Fuel Cells*, vol. 13, no. 4, pp. 487–493, 2013, doi: 10.1002/fuce.201200180.
[36] K. W. Reeping, J. M. Bohn, and R. A. Walker, “Palliative effects of H2 on SOFCs operating with carbon containing fuels,” *J. Power Sources*, vol. 372, pp. 188–195, Dec. 2017, doi: 10.1016/j.jpowsour.2017.10.071.
[37] E. Dogdibegovic, Y. Cheng, F. Shen, R. Wang, B. Hu, and M. C. Tucker, “Scaleup and manufacturability of symmetric-structured metal-supported solid oxide fuel cells,” *J. Power Sources*, vol. 489, p. 229439, Mar. 2021, doi: 10.1016/j.jpowsour.2020.229439.
[38] M. M. Welander, B. Hu, and M. C. Tucker, “Metal-supported solid oxide fuel cells operating with reformed natural gas and sulfur,” *Int. J. Hydrog. Energy*, vol. 47, no. 21, pp. 11261–11269, Mar. 2022, doi: 10.1016/j.ijhydene.2022.01.170.
[39] H. A. Shabri, M. H. D. Othman, M. A. Mohamed, T. A. Kurniawan, and S. M. Jamil, “Recent progress in metal-ceramic anode of solid oxide fuel cell for direct hydrocarbon fuel utilization: A review,” *Fuel Process. Technol.*, vol. 212, p. 106626, Feb. 2021, doi: 10.1016/j.fuproc.2020.106626.
[40] E. P. Murray, S. J. Harris, J. Liu, and S. A. Barnett, “Direct Solid Oxide Fuel Cell Operation Using a Dimethyl Ether/Air Fuel Mixture,” *Electrochem. Solid-State Lett.*, vol. 8, no. 10, p. A531, Aug. 2005, doi: 10.1149/1.2033622.
[41] C. Su, R. Ran, W. Wang, and Z. Shao, “Coke formation and performance of an intermediate-temperature solid oxide fuel cell operating on dimethyl ether fuel,” *J. Power Sources*, vol. 196, no. 4, pp. 1967–1974, Feb. 2011, doi: 10.1016/j.jpowsour.2010.10.011.
[42] A. E. Richards, M. G. McNeeley, R. J. Kee, and N. P. Sullivan, “Gas transport and internal-reforming chemistry in Ni–YSZ and ferritic-steel supports for solid-oxide fuel cells,” *J. Power Sources*, vol. 196, no. 23, pp. 10010–10018, Dec. 2011, doi: 10.1016/j.jpowsour.2011.07.086.
[43] M. D. McIntyre, D. M. Neuburger, and R. A. Walker, “In Situ Optical Studies of Carbon Accumulation with Different Molecular Weight Alkanes on Solid Oxide Fuel Cell Ni Anodes,” *ECS Trans.*, vol. 66, no. 32, pp. 11–19, Jul. 2015, doi: 10.1149/06632.0011ecst.
[44] M. C. Tucker, “Durability of symmetric-structured metal-supported solid oxide fuel cells,” *J. Power Sources*, vol. 369, pp. 6–12, Nov. 2017, doi: 10.1016/j.jpowsour.2017.09.075.